Journal of Medical Ultrasonics (2019) 46:377–388
https://doi.org/10.1007/s10396-019-00962-2

ORIGINAL ARTICLE–PHYSICS & ENGINEERING

# Inhibition of myostatin signal pathway may be involved in low-intensity pulsed ultrasound promoting bone healing

**Lijun Sun[1] · Shuxin Sun[2] · Xinjuan Zhao[1] · Jing Zhang[1] · Jianzhong Guo[3] · Liang Tang[1] · Dean Ta[2,4,5]**

Received: 22 March 2019 / Accepted: 12 June 2019 / Published online: 3 August 2019


## Abstract

**Purpose** Low-intensity pulsed ultrasound (LIPUS) is effective in promoting bone healing, and a myostatin deficiency also has a positive effect on bone formation. In this study, we evaluated the effects of LIPUS on bone healing in rats in vivo and investigated the mechanisms in vitro, aiming to explore whether LIPUS promotes bone healing through inhibition of the myostatin signaling pathway.

**Methods** Rats with both drill-hole defects and MC3T3-E1 cells were randomly assigned to a LIPUS group and a control group. The LIPUS group received LIPUS treatment (1.5 MHz, 30 mW/cm$^2$) for 20 min/day.

**Results** After 21 days, the myostatin expression in quadriceps was significantly inhibited in the LIPUS group, and remodeling of the newly formed bone in the drill-hole site was significantly better in the LIPUS group than that in the control group, which was confirmed by micro-CT analysis. After 3 days, LIPUS significantly promoted osteoblast proliferation; inhibited the expression of AcvrIIB (the myostatin receptor), Smad3, p-Smad3, and GSK-3β; and increased Wnt1 and β-catenin expression. Moreover, translocation of β-catenin from the cytolemma to the nucleus was observed in the LIPUS group. However, these effects were blocked by treatment with myostatin recombinant protein.

**Conclusions** The results indicate that LIPUS may promote bone healing through inhibition of the myostatin signal pathway.

**Keywords** Low-intensity pulsed ultrasound · Bone healing · Bone micro-architectures · Proliferation · Myostatin · Wnt

## Introduction

Millions of fractures occur annually worldwide; a significant percentage of fractured bones experience delayed healing and in some cases result in a non-union. Bone formation and regeneration is a complex physiological process that sequentially involves chemotaxis, cell proliferation, cell differentiation, and the synthesis of extracellular matrix as a result of interactions among biochemical, biomechanical, cellular, and hormonal signals [1]. Ultrasound is not only used for diagnosis [2, 3] but also for treatment. Low-intensity pulsed ultrasound (LIPUS) has been reported to promote the healing of fresh fractures, non-union, and delayed union in animal models and clinical treatment [4-7]. LIPUS stimulation is a clinically established, widely used treatment for accelerating bone fracture healing that has been approved by the U.S. Food and Drug Administration (FDA) [8]. As a very mild mechanical stimulation, LIPUS produces pressure waves that are transmitted into the tissues as high-frequency acoustic pressure waves that cause biochemical events

Lijun Sun, Shuxin Sun and Xinjuan Zhao contributed equally to this work and should be regarded as co-first authors.

✉ Liang Tang
tl531@snnu.edu.cn

✉ Dean Ta
tda@fudan.edu.cn

1 Institute of Sports Biology, Shaanxi Normal University, Xi'an 710119, China

2 Department of Electronic Engineering, Fudan University, Shanghai 200433, China

3 Shaanxi Key Laboratory of Ultrasonics, Shaanxi Normal University, Xi'an 710119, China

4 Human Phenome Institute, Fudan University, Shanghai 201203, China

5 Key Laboratory of Medical Imaging Computing and Computer Assisted Intervention (MICCAI) of Shanghai, Shanghai 200032, China

at the cellular level. LIPUS promotes cell proliferation, pre-conditions cells to orient their differentiation during culture [9-11], and transfects cells [12]. Bone cells are sensitive to strain, as reported previously [13, 14]. The micro-mechanical stress produced by LIPUS causes bone mechanoreceptors to convert biophysical stimuli into biochemical responses that alter gene expression and cellular adaptation [15]. However, the specific underlying cellular and molecular mechanisms of LIPUS on bone healing are still unclear.

Myostatin, a member of the transforming growth factor (TGF)-β super-family, is a highly conserved protein secreted primarily from skeletal muscle that can potently suppress skeletal muscle growth [16]. Myostatin mutations in animals or humans result in a dramatic increase in skeletal muscle mass and strength [17, 18]. Although myostatin is expressed in skeletal muscle, it can also circulate as an endocrine factor [19]. Myostatin is one of the key factors linking muscle and bone. The physiological effects of myostatin deletion are not restricted to strengthened skeletal muscle, but also include enhanced bone formation. Myostatin-knockout mice showed increased bone mineral density (BMD) compared to their wild-type counterparts [20]. Increased whole-body BMD and bone mineral content (BMC) were found to persist into old age in myostatin-knockout mice [21-23]. Serum levels of myostatin-immunoreactive protein have been observed to increase with age [24], suggesting that altered myostatin signaling may play a role in the loss of muscle and bone mass that accompanies aging in musculoskeletal tissues. Our previous study also showed that blocking myostatin using a prepared polyclonal antibody prevented bone loss in diet-induced obese rats [25].

Although osteoblasts do not express and secrete myostatin, a myostatin receptor, the activin type IIB receptor (AcvrIIB), is expressed in osteoblasts in the tibiae of neonatal rats [26]. Hamrick et al. identified that signaling through AcvrIIB may alter the mechanosensitivity of bone marrow stromal cells and is involved in bone modeling [27]. The Wnt/β-catenin signaling pathway has been reported to regulate osteoblast activities and control bone mass, and β-catenin is a key molecule of the canonical Wnt/β-catenin signaling pathway [28-30]. Glycogen synthase kinase-3β (GSK3-β) phosphorylated β-catenin, triggering its destabilization and degradation to maintain a very low level of β-catenin in the cytosol/nucleus [31]. Recombinant mouse myostatin was reported to specifically induce Smad3 phosphorylation and stabilize β-catenin during the differentiation programs of bone marrow-derived mesenchymal stem cells and brown adipocytes [32, 33]. Taken together, the downstream signaling molecules of myostatin, including AcvrIIB and Smad3, play an important role in the regulation of bone formation and are directly involved in the enhancement of β-catenin levels. Therefore, it is hypothesized that LIPUS might promote bone healing through inhibition of the myostatin signal pathway.

In the present study, the effect of LIPUS on bone healing in rats in vivo was verified by observing new bone formation in the drill-hole site of femurs using micro-CT. Furthermore, its mechanisms were investigated by assessing the myostatin expression in muscle and the effects of LIPUS and myostatin recombinant protein on the proliferation of MC3T3-E1 cells, and analyzing the related gene and protein expressions of Wnt and myostatin signal pathway in osteoblasts in vitro.

## Materials and methods

### Animals and surgery

Sixteen healthy female Sprague–Dawley rats weighing 200–250 g were purchased from the Laboratory Animal Breeding and Research Center of Xi'an Jiao tong University (Xi'an, China). The rats were housed in a controlled room (22 ± 2 °C, 60 ± 5% humidity, and 12-h light/dark cycle) and fed a standard laboratory diet and water. In this study, after general anesthesia was established with sodium pentobarbital (30 mg/kg intraperitoneally), the surgical area was shaved and the skin was washed with 70% ethanol. A skin incision was made on the lateral side of the right femur. The quadriceps femoris was bluntly cut to expose the femoral diaphysis. A 1-mm-diameter drill was then used to produce a 1-mm-diameter perforation through the anterior cortices. The hole was rinsed by an injection of saline to remove bone fragments from the cavity. The muscles were subsequently repositioned, and the skin was closed with suture. Animals were randomly allocated to two groups (8 in each group): control group (sham-treated group) and LIPUS group. Within the first 72 h, the animals did not receive any treatment. Animal care and experimental procedures were approved by the Animal Ethical Committee of Shaanxi Normal University, and carried out in accordance with the National Institutes of Health Guide for the Care and Use of Laboratory Animals (NIH Publications No. 8023, revised in 1978).

### Cell culture

Mouse calvarial osteoblast cell line MC3T3-E1 cells were obtained from Xi'an Jiaotong University (Xi'an, China). The cells were cultured in a growth medium consisting of Dulbecco's modified Eagle's medium (DMEM; HyClone, USA) containing 10% (v/v) fetal bovine serum (FBS; HyClone, USA) and 1% (v/v) penicillin–streptomycin solution (50 U/mL penicillin and 50 µg/mL streptomycin; HyClone, USA) at 37 °C in a humidified atmosphere with 5% $CO_2$. The medium was changed every 3 days. When 80% confluence was reached, the attached cells were digested with 0.25%

trypsin/EDTA (HyClone, USA) and replated for further expansion.

## LIPUS treatment

The LIPUS device (Department of Electronic Engineering, Fudan University) produced a 200-μs burst of 1.5 MHz acoustic sine waves with a spatial-averaged temporal-averaged intensity ($I_{SATA}$) of 30 mW/cm$^2$ repeating at 1000 Hz. A kind of plane circular transducer, 25 mm in diameter, was used for this experiment, and the intensity was calibrated by a high-resolution (1 mW) ultrasound power meter (UPM-DT-1000PA; Ohmic Instruments, MO, USA). The ultrasound power meter is designed to measure the ultrasound power output of medical ultrasonic transducers using the radiation force balance method, which is the most reliable and repeatable means of measuring ultrasound power. In detail, the intensity of a transducer is determined by measuring the total power output and dividing by the active cross-sectional area of the transducer. In the LIPUS group, the culture plates were placed on the ultrasound transducers with a thin layer of ultrasonic coupling gel between them and exposed to ultrasound for 20 min/day for 3 days. Three days after drilling, the right femurs of the rats in the LIPUS group were exposed to LIPUS for 20 min/day for 3 weeks. In both in vitro and in vivo experiments, the control group received sham ultrasound stimulation.

## Micro-CT analysis

The 3D image and bone volume over total volume (BV/TV) of mineralized bone formation in the drill-hole site were evaluated using micro-CT (ZKKS-MCT-Sharp; Beijing, China). The scanning system was set to 50 kV and 50 W. The scanning resolution was 35 μm/slice. Scanned images were reconstructed and analyzed using 3D Med analysis software version 4.5 (Key Laboratory of Molecular Imaging, Chinese Academy of Sciences, Beijing, China).

## Immunohistochemistry analysis

Serial sections (thickness 8–10 μm) of muscle tissues were frozen sections transferred to impregnated slides and fixed for 10 min by acetone. The sections were incubated with 3% $H_2O_2$ diluted in methanol for 20 min, blocking buffer (3% BSA in PBS) for 30 min, and purified anti-myostatin monoclonal antibody (1:50) for 1 h in turn. The washed sections were then incubated with an HRP-coupled IgG (1:150; Santa Cruz, CA, USA) for 30 min, followed by a DAB/peroxidase reaction (0.006% $H_2O_2$, 0.05 mg/mL DAB) until the color was detected. PBS replaced the primary antibody as a negative control. Quantitative analysis of immunohistochemistry was performed with Image-pro plus 6.0 using the standard acquisition camera mode (20× objective) (Thermo Scientific, USA).

## Cell counting kit-8 assays

The cell viability was evaluated using the Cell Counting Kit-8 reagents (Dojindo Laboratories, Japan). Briefly, 10 μL of Cell Counting Kit-8 solution were added to each well containing 100 μL medium, and then the cells were incubated for 2 h at 37 °C in the dark. The absorbency was measured at 450 nm using a microplate reader (BIO-RAD Laboratories, Hercules, CA, USA). The cell survival rate was then calculated according to the instructions. There were six wells per group and the experiment was repeated three times.

## Quantitative RT-PCR

Total cellular RNA was isolated by Trizol reagent (Invitrogen, Carlsbad, CA, USA) according to the manufacturer's instructions and then reverse-transcribed using a PrimeScript™ II 1st Strand cDNA Synthesis Kit (Takara Shuzo, Shiga, Japan). RNA was denatured at 65 °C for 5 min, followed by cDNA synthesis at 42 °C for 1 h. The reaction was stopped at 95 °C for 5 min. The expression of genes was analyzed by the CFX96 Real-Time PCR Detection System (BIO-RAD Laboratories). All real-time PCR reactions were performed in triplicate, and the gene expression levels were normalized by dividing the calculated values for the mRNA samples by that of glyceraldehyde-3-phosphate dehydrogenase (GAPDH) mRNA at each time point. The relative change in gene expression was analyzed by the $2-\triangle\triangle$CT method. The primers used were as follows: TGGTGACAGGGAAGACATCA (forward) and CCACAA CAGGCAGTCCATAA (reverse) for β-catenin, AGGAGA AGTGGTGCGAGAG (forward) and GTGACCTGGGGA TGGTAATG (reverse) for Smad3, GATTATCACGCTACC ACG (forward) and ATTCAGCCCATCTTCTCC (reverse) for Myostatin, and TTTGAGGGTGCAGCGAACTT (forward) and ACAGCAACAGGGTGGTGGAC (reverse) for GAPDH.

## Western blot analysis

Cultured cells were washed three times with ice-cold phosphate buffered saline (PBS) containing 1 mM sodium orthovanadate and harvested in ice-cold RIPA buffer containing a protease inhibitor and phosphatase inhibitor cocktail (Beijing Dingguo Changsheng Biotech, Beijing, China). Protein concentrations were measured with a BCA protein assay kit (Beijing Dingguo Changsheng Biotech). The immunoblots were incubated with primary antibodies overnight at 4 °C, followed by incubation with the corresponding secondary horseradish peroxidase

(HRP)-conjugated goat anti-mouse or anti-rabbit IgG (diluted 1:5000) (Cell Signaling Technology, Boston, USA) at room temperature for 1 h. The blots were visualized with ECL-plus reagent and the results were quantified by Lab Image version 2.7.1. The following primary antibodies were used: myostatin (EPR4567(2), ab124721), ActRIIB (EPR10739, ab180185), and Wnt1 (ab15251) from Abcam, and Smad2/3 (5678S), β-Catenin (8480S), GSK-3β (59558S), phospho-Smad2/3 (8828S), and phospho-Smad3 (9520S) from Cell Signaling Technology.

### Inhibitor treatment

MC3T3-E1 cells were seeded in 96-well plates and 6-well plates at a density of $2\times10^4$ cells/well and $1\times10^6$ cells /well, respectively, and then maintained in DMEM containing 10% FBS for 24 h until they were adherent. The medium was then changed to DMEM supplemented with or without myostatin recombinant protein (50 ng/mL) (Recombinant Mouse GDF 8/Myostatin, Catalog No. 788-G8; R&D Systems, Minneapolis, MN, USA). Cells were randomly divided into the following groups: control group (cultured with DMEM for 72 h), LIPUS group (cultured with DMEM for 72 h and treated with LIPUS for 20 min/day), and LIPUS + myostatin group (cultured with DMEM supplemented with myostatin recombinant protein for 72 h and treated with LIPUS for 20 min/day). After the treatment, the cell proliferation was analyzed using Cell Counting Kit-8 reagents (Dojindo Laboratories, Japan), and the RNA and protein of MC3T3-E1 cells were extracted to detect the expression of related molecules.

### Immunofluorescence analyses

The cells, grown on circular glass coverslips in 24-well plates, were washed in PBS and fixed with 4% paraformaldehyde in PBS for 15 min. The plasma membranes were permeabilized in PBS containing 0.5% Triton X-100 for 20 min. Coverslips were incubated in a blocking buffer (1% BSA in PBS) before leaving them overnight at 4 °C with the primary antibody, anti-β-catenin. After washing with PBS, the cells were incubated with goat anti-rabbit FITC (1:100; Boster Biological Technology, Pleasanton, CA, USA) for 1 h in the dark at 37 °C. Nuclei were counterstained with Hoechst 33,258 (1:3000) (Sigma-Aldrich, St. Louis, MO, USA) for 20 min. The results were observed with a fluorescence microscope (Nikon Eclipse 55i; Nikon, Tokyo, Japan). Quantitative analysis of immunofluorescence was performed with a Cellomics® Arrayscan VTI HCS Reader using the standard acquisition camera mode (20× objective) (Thermo Scientific, Waltham, MA, USA).

### Statistical analysis

All statistical analyses were performed using SPSS 17.0 software (SPSS, Chicago, IL, USA). The data were expressed as the mean ± standard deviation (SD) and were analyzed using one-way ANOVA and Tukey's multiple comparisons seeking to identify statistically significant differences between every two groups. A $p$ value $< 0.05$ was considered statistically significant.

## Results

### Micro-CT analysis for bone healing in vivo

The positive effects of the LIPUS treatment on bone regeneration in the drill-hole site of rat femurs were supported by 3D micro-CT, as shown in Fig. 1. In both the control and LIPUS groups, modestly mineralized calluses appeared at the defect region 7 days after the drill-hole surgery. At day 14, the extent of callus mineralization was increased, and the defect region was partially bridged. At day 21, the mineralized callus within the defect region was completely bridged. The remodeling of newly formed bone at the cortical bone gap was significantly greater in the LIPUS group than in the control group from day 14 to day 21 (Fig. 1a, b). Compared with the control group, the BV/TV in the drill-hole site was significantly higher in the LIPUS group at day 14 ($p < 0.05$) and day 21 ($p < 0.01$) (Fig. 1c).

### The effect of LIPUS on myostatin expression in quadriceps

To investigate the effect of LIPUS on myostatin, an important link between muscle and bone, the myostatin expression in quadriceps was detected (Fig. 2). The gene ($p < 0.05$) and protein ($p < 0.05$) expressions of myostatin were significantly down-regulated in the LIPUS group compared with the control group. Immunohistochemistry analysis results showed that 3 weeks of LIPUS treatment significantly reduced the integrated optical density (IOD) of myostatin compared with the sham-treated rats ($p < 0.05$).

### The effect of LIPUS on related protein expressions of Wnt and myostatin signal pathway in MC3T3-E1 cells

The protein expressions of AcvrIIB, Smad2/3, pSmad2/3, Wnt1, GSK-3β, and β-catenin in MC3T3-E1 cells were measured by western blotting. As shown in Fig. 3, after LIPUS stimuli for 3 days, the protein expressions of β-catenin ($p < 0.05$) and Wnt1 ($p < 0.05$) were significantly higher than in the control group. The protein expressions of AcvrIIB

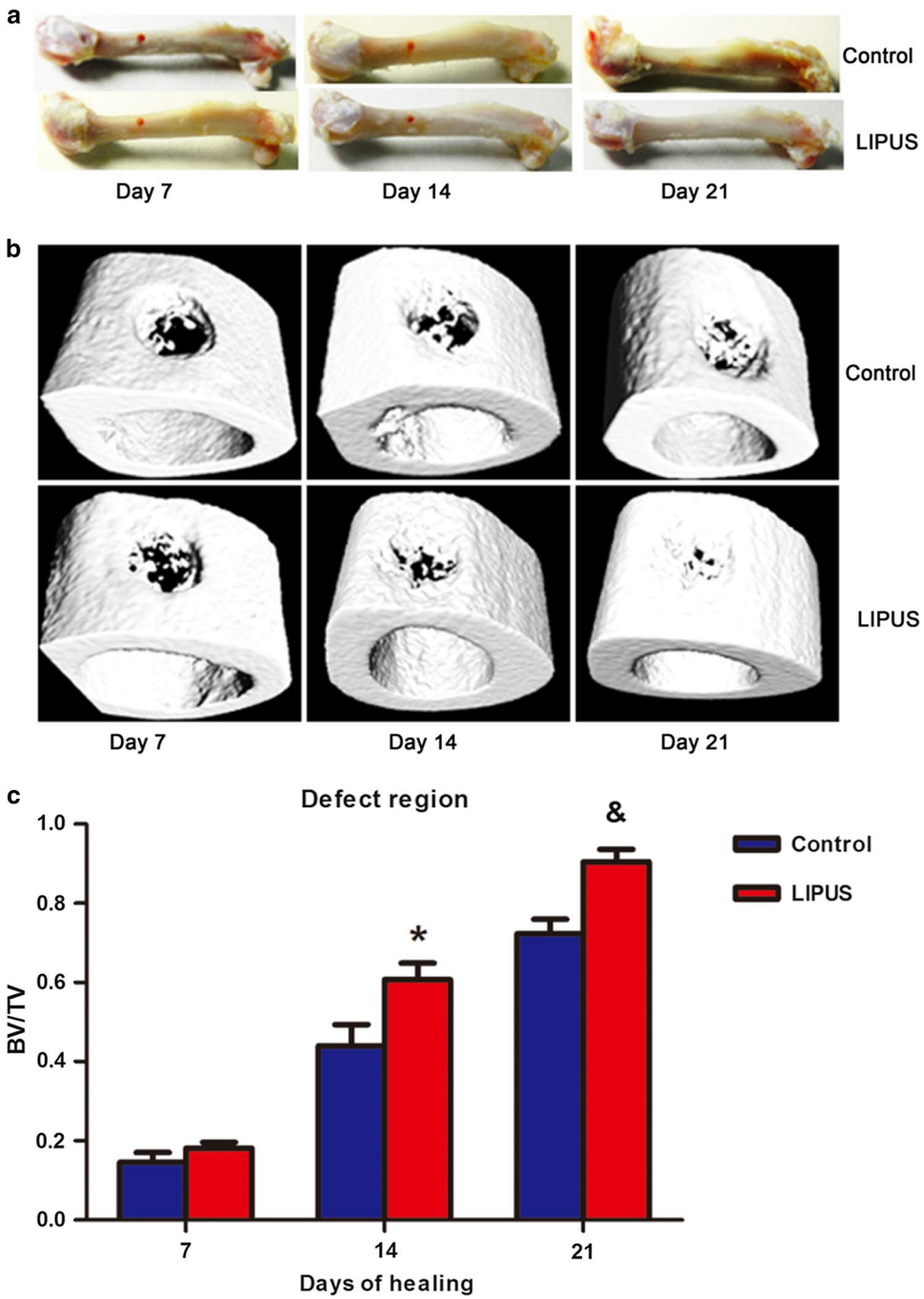


**Fig. 1** 3D reconstruction and BV/TV of mineralized bone formation in the drill-hole site of rat femurs at days 7, 14 and 21. **a** Pictures of whole bones with drilled hole. **b** 3D reconstruction of new bone in the drill-hole site. **c** BV/TV of mineralized bone formation in the drill-hole site. &$p < 0.01$ vs. control group, *$p < 0.05$ vs. control group

($p < 0.01$), Smad3 ($p < 0.05$), pSmad3 ($p < 0.05$), and GSK-3β ($p < 0.01$) were all significantly decreased in the LIPUS group compared with the control group, whereas the protein expressions of Smad2 and pSmad2 were not significantly different between the two groups.

## The effect of LIPUS on β-catenin translocation to the nucleus in MC3T3-E1 cells

β-catenin, which is an inducible transcription factor, localizes to the cytolemma as a compound. It regulates

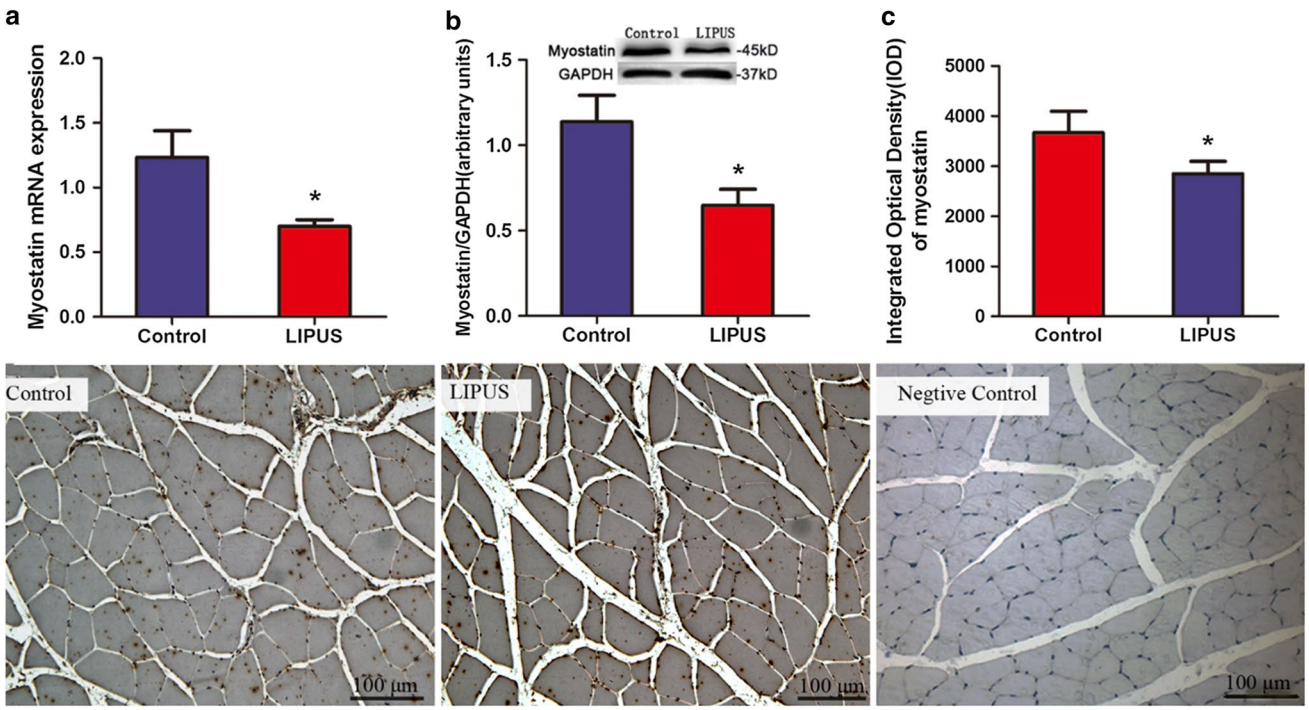


**Fig. 2** The effect of LIPUS on myostatin expression in quadriceps. **a** The protein expression of myostatin **b** the gene expression of myostatin, and **c** statistical results for immunohistochemistry analysis. The data are expressed as the mean ± SD. *$p < 0.05$ vs. control group. Bar is 100 μm

osteoblast proliferation when it transfers to the nucleus. The translocation of β-catenin from the cytolemma to the nucleus was observed after 3 days of LIPUS stimulation (Fig. 4). Qualitatively, the LIPUS group had more extensive nuclear and perinuclear signals of β-catenin in MC3T3-E1 cells. Quantitative measurements indicated that the LIPUS group had a significantly higher positive average intensity ($p < 0.05$) and area fraction ($p < 0.05$) of cells exhibiting nuclear or perinuclear β-catenin staining than that of the control group, as shown in Fig. 4d.

## The effect of myostatin recombinant protein on proliferation of MC3T3-E1 cells treated with LIPUS

To clarify the role of the myostatin signal pathway in the promotion of osteoblast proliferation induced by LIPUS, we examined the effect of LIPUS on the proliferation of MC3T3-E1 cells in the presence of myostatin recombinant protein. As shown in Fig. 5, LIPUS significantly promoted the proliferation of MC3T3-E1 cells compared with the control group ($p < 0.01$). However, compared with the LIPUS group, the OD values of the LIPUS + myostatin group were significantly down-regulated ($p < 0.05$).

## The effect of myostatin recombinant protein on Smad3 and β-catenin expressions in MC3T3-E1 cells treated with LIPUS

To further determine the downstream molecules of the myostatin signal pathway in LIPUS-induced osteoblast proliferation, we detected β-catenin and Smad3 expression response to LIPUS in the presence of myostatin recombinant protein. As shown in Fig. 6a, b, the gene ($p < 0.05$) and protein (− 14%, $p = 0.067$) expressions of β-catenin were all decreased in the LIPUS + myostatin group compared with the LIPUS group. The gene expression ($p < 0.05$) and protein phosphorylation ($p < 0.05$) of Smad3 were all significantly increased in the LIPUS + myostatin group compared with the LIPUS group (Fig. 6c, d). It demonstrated that LIPUS promoted the osteoblast proliferation by modulation of Smad3-induced β-catenin stabilization and that Smad3 is a key molecule in LIPUS promoting osteoblast proliferation through inhibiting the myostatin signal pathway.

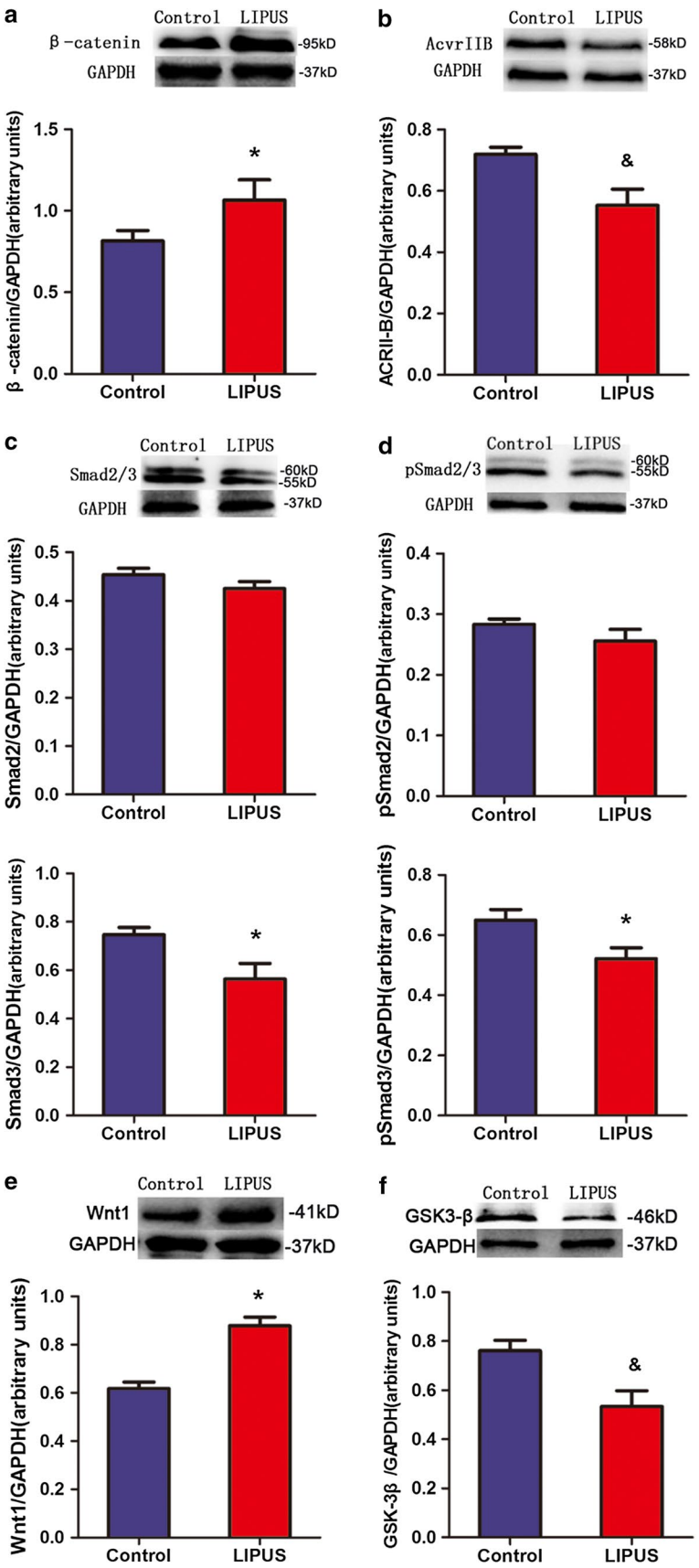


**Fig. 3** The effect of LIPUS on related protein expression of Wnt and the myostatin signal pathway in MC3T3-E1 cells. **a** β-catenin, **b** AcvrIIB, **c** Smad2/3, **d** phosphorylated Smad2/3 (pSmad2/3), **e** Wnt1, **f** GSK-3β. The blots were quantified using Image J. Data are mean ± SD ($n = 6$ per group). &$p < 0.01$ vs. control group, *$p < 0.05$ vs. control group

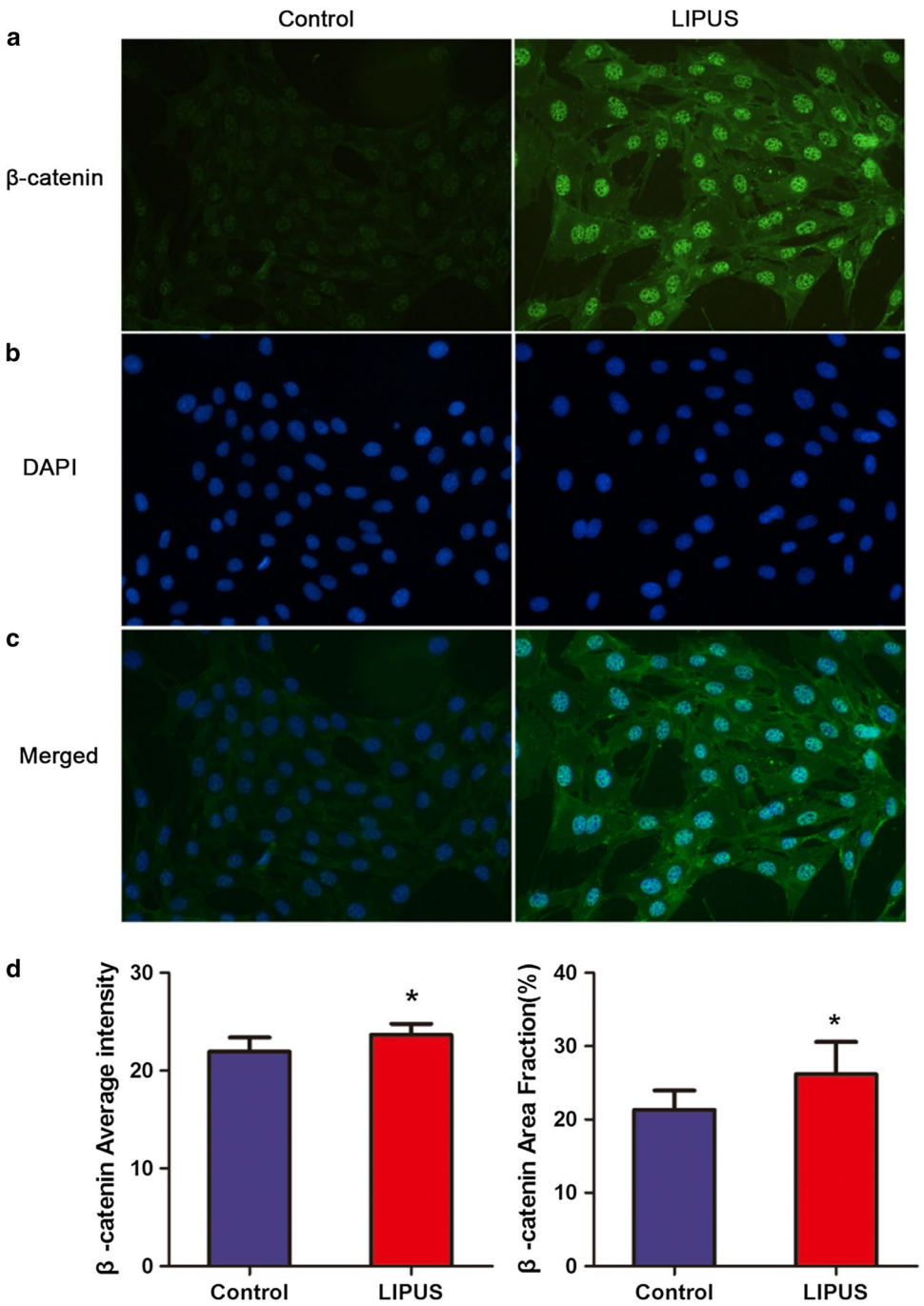


**Fig. 4** The translocation of β-catenin in MC3T3-E1 cells after LIPUS treatments (×200). Cells were treated with 20 min/day for 3 days and stained with fluorescent antibodies against **a** β-catenin (green) **b** DAPI (blue), and **c** combination of β-catenin and DAPI. **d** The β-catenin average intensity and area fraction. *$p < 0.05$ vs. control group

## Discussion

Millions of fractures occur annually worldwide; approximately 5–10% of all fractures experience delayed healing, and some even result in a non-union [1]. LIPUS was found to play a positive role in enhancing fracture healing in various in vivo and in vitro studies [4-7]. On the other hand, there is growing evidence that myostatin inhibition plays an important role in increasing BMD and bone formation [20, 21]. Whether LIPUS promotes bone healing through the inhibition of the myostatin signal pathway has been poorly studied. Our results demonstrated that LIPUS may promote bone healing through decreasing the myostatin expression in muscle and inhibiting the myostatin signal pathway in osteoblasts including down regulating AcvrIIB and Smad3, and activing β-catenin.

As a new high-resolution digital imaging technique, micro-CT is considered a useful and reliable method for evaluating bone healing [34]. Defective bone microstructure parameters could be improved by LIPUS, as reported

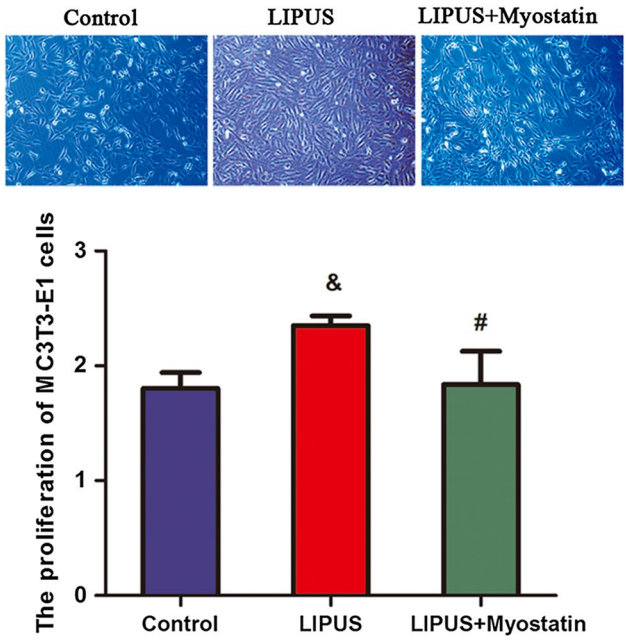


**Fig. 5** The effect of myostatin recombinant protein on the proliferation of osteoblasts treated with LIPUS. Effect of LIPUS and myostatin on the proliferation of osteoblasts. The data are expressed as the mean ± SD. &$p < 0.01$ vs. control group, #$p < 0.05$ vs. LIPUS group

previously [35, 36]. Sakurakichi et al. found larger callus formation, higher BMD, and a correspondingly higher biomechanical stiffness and strength in a LIPUS group [37, 38]. Similarly, Tis et al. reported that the BMD, BMC, and bone strength index were significantly increased within the period of bone remodeling in a LIPUS group [39]. Furthermore, Heckman et al. demonstrated a 38% reduction in the healing time of tibia fractures using LIPUS [4]. Similarly, Kristiansen et al. found a 30% acceleration in fractures of the distal radius using LIPUS [5]. In the present study, consistent with these findings, our results also demonstrated that LIPUS could accelerate bone healing in a rat femoral osteotomy model, as confirmed by micro-CT analysis. After 3 weeks of LIPUS treatment, the extent of callus mineralization and the volume of mineralized callus were higher in the LIPUS group than in the control group. The positive effects of LIPUS treatment on bone regeneration were further supported by 3D Micro-CT images. The Micro-CT scan results confirmed that LIPUS was an effective modality for accelerating bone regeneration and shortening the healing time.

Myostatin, a key negative regulator of muscle, is expressed in skeletal muscle, but it can also circulate to target organs as an endocrine factor [19]. Among the target organs, bone is the most important organ modulated by myostatin. As a key factor linking muscle and bone, myostatin deficiency has a positive effect on bone formation [20-23]. Our previous experiments also showed that the ladder climbing exercise did not only reduce the myostatin expression in muscle but also decreased the concentration of myostatin in serum in obese rats, and then reversed obesity-induced bone loss [40, 41], suggesting that the content of myostatin in serum was positively correlated with the expression of myostatin in skeletal muscle. Our previous

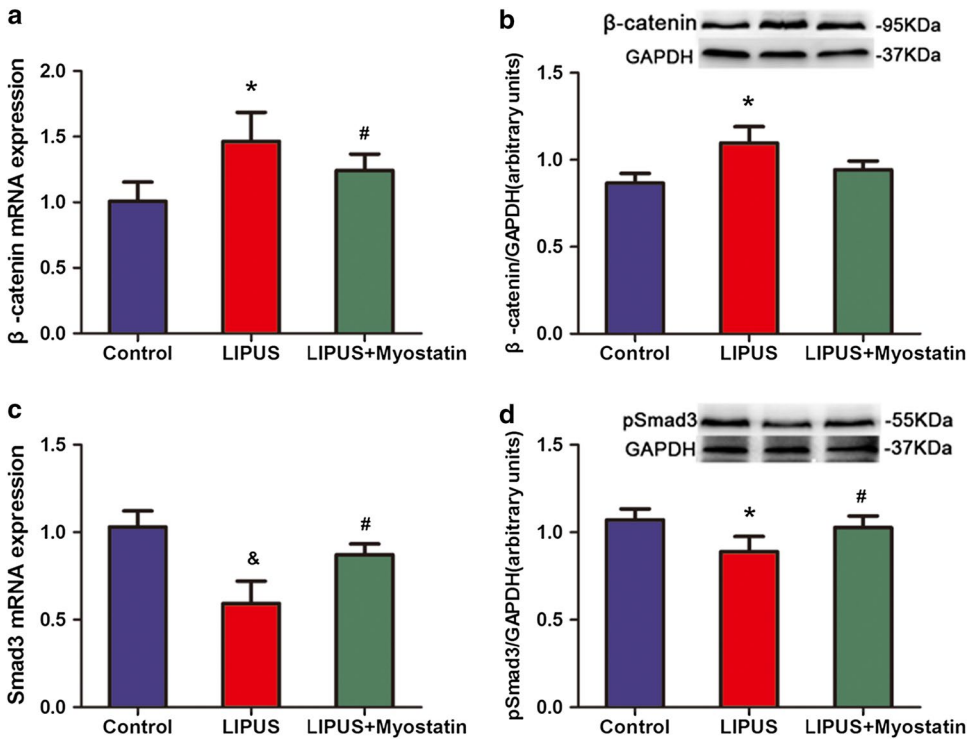


**Fig. 6** The effect of myostatin recombinant protein on Smad3 and β-catenin expressions in MC3T3-E1 cells treated with LIPUS. **a** The gene expression of β-catenin **b** the protein expression of β-catenin **c** the gene expression of Smad3, and **d** the protein expression of Smad3. The data are expressed as the mean ± SD. *$p < 0.05$, &$p < 0.01$, #$p < 0.05$

studies demonstrated that LIPUS could promote exercise-induced muscle hypertrophy and prevent muscle atrophy induced by type 1 diabetes through inhibiting the expression of myostatin [42, 43]. Like the previous study, in the present study, LIPUS treatment significantly down-regulated the expression of myostatin in quadriceps, so it can be inferred that the content of myostatin in serum must be decreased. Therefore, inhibiting myostatin by LIPUS in muscle may be involved in promoting the process of bone healing.

Since the amount of osteoblasts in bone tissue is very small (even smaller at the defect site), it is difficult to determine the downstream molecules of the myostatin signal pathway involved in LIPUS accelerating bone healing in vivo. Thus, in this study, the ME3T3-E1 osteoblastic cell line was selected to further investigate the mechanisms by which LIPUS promotes bone healing in vitro. Osteoblasts play an important role in the process of bone formation. Recently, many researchers have focused on a more comprehensive understanding of the cellular and molecular mechanisms of LIPUS on osteoblasts. The proliferation of osteoblasts was increased when ultrasound stimulation was performed with a low-pulse repetition frequency and short exposure time, as reported previously [44, 45]. Zhou et al. attributed LIPUS-induced cell proliferation to the activation of integrin receptors [46]. Tis et al. [39] reported that the osteoblast cell counts were significantly increased after LIPUS treatment. Similar positive effects of LIPUS were observed by Lim [47]. In accordance with these findings, our results also demonstrated that LIPUS stimulation significantly enhanced the proliferation of ME3T3-E1 cells. Furthermore, the Wnt/β-catenin signaling pathway, which plays an important role in the differentiation and proliferation of osteoblasts, has been identified as one of the cellular reactions activated by the mechanical stimulation [48]. Fung et al. depicted β-catenin nuclear translocation in LIPUS-stimulated osteocytes [49]. In accordance with the previous findings, the immunofluorescence results of the present study also showed that LIPUS could promote the translocation of β-catenin into the nuclei of ME3T3-E1 cells. Moreover, the expression of β-catenin and Wnt1 was significantly up-regulated, and the GSK-3β expression was down-regulated after the LIPUS treatment. However, the positive effects of LIPUS on both the proliferation of osteoblasts and the translocation of β-catenin were blocked by myostatin recombinant protein. Taken together, these results indicated that acceleration of osteoblast proliferation through the Wnt/β-catenin signaling pathway was involved in LIPUS promoting bone healing, which may be regulated by myostatin signal pathways.

As the myostatin receptor, the type IIB activin receptor (AcvrIIB) is expressed in osteoblasts [26], although osteoblasts do not express myostatin. Hamrick et al. identified that signaling through AcvrIIB might alter the mechanosensitivity of bone marrow stromal cells and was involved in bone modeling [27]. It was reported that the binding of myostatin to AcvrIIB resulted in phosphorylation of smad2/3 [50]. Egerman et al. also reported that myostatin could induce Smad2/3 phosphorylation [51], leading to inhibition of the expression of Runx2 as a critical activator of osteogenesis [52, 53]. As the downstream signaling molecules of myostatin, AcvrIIB, Smad2, and Smad3 were all reported to play an important role in the regulation of bone formation and be directly involved in the enhancement of β-catenin levels [54, 55]. Moreover, Lei et al. demonstrated that LIPUS was associated with downregulation of the protein expression of phospho-Smad2/3 and Smad2/3 in penile tissue [56]. Therefore, we speculated that LIPUS might promote osteoblast proliferation at bone defects by inhibiting the downstream molecules of myostatin. In this study, our results showed that the expressions of AcvrIIB, Smad3, and pSmad3 were dramatically down-regulated in MC3T3-E1 cells after LIPUS treatment. However, when myostatin recombinant protein was added, the inhibition of pSmad3 induced by LIPUS was totally negated, while the osteoblast proliferation promoted by LIPUS was significantly inhibited. The results indicated that Smad3 was a key molecule in LIPUS promoting osteoblast proliferation by inhibiting the myostatin signal pathway.

## Conclusions

The present study is the first report demonstrating that LIPUS may promote bone healing by decreasing the myostatin expression in muscle and inhibiting the myostatin signal pathway in osteoblasts. The finding in this study provides a theoretical basis for the application of LIPUS in medical practice and additional evidence for the direct effect of myostatin on bone formation.

**Acknowledgements** This work was supported by the National Natural Science Foundation of China (Nos. 11827808, 11774213, 11727813, 11502134, and 11525416), the Natural Science Foundation of Shaanxi Province (2018JM1022), the Fundamental Research Funds for the Central Universities (GK201703092 and GK201703091), and Shanghai Municipal Science and Technology Major Project (2017SHZDZX01).

### Compliance with ethical standards

**Conflict of interest** The authors declare that they have no competing interests.

**Ethical statements** Animal care and experimental procedures were approved by the Animal Ethical Committee of Shaanxi Normal University, and carried out in accordance with the National Institutes of Health Guide for the Care and Use of Laboratory Animals (NIH Publication No. 8023, revised in 1978).

## References


1. Bolander ME. Regulation of fracture repair by growth factors. Proc Soc Exp Biol Med. 1992;200:165–70.
2. Tran T, Le LH, Sacchi MD, Nguyen VH. Sensitivity analysis of ultrasonic guided waves propagating in trilayered bone models: a numerical study. Biomech Model Mechanobiol. 2018;17:1267–79.
3. Schone M, Schulz RM, Tzschatzsch H, Varga P, Raum K. Ultrasound palpation for fast in-situ quantification of articular cartilage stiffness, thickness and relaxation capacity. Biomech Model Mechanobiol. 2017;16:1171–85.
4. Heckman JD, Ryaby JP, McCabe J, Frey JJ, Kilcoyne RF. Acceleration of tibial fracture-healing by non-invasive, low-intensity pulsed ultrasound. J Bone Jt Surg Am. 1994;76:26–34.
5. Kristiansen TK, Ryaby JP, McCabe J, Frey JJ, Roe LR. Accelerated healing of distal radial fractures with the use of specific, low-intensity ultrasound A multicenter, prospective, randomized, double-blind, placebo-controlled study. J Bone Jt Surg Am. 1997;79:961–73.
6. Mayr E, Frankel V, Ruter A. Ultrasound–an alternative healing method for nonunions? Arch Orthop Trauma Surg. 2000;120:1–8.
7. Takikawa S, Matsui N, Kokubu T, Tsunoda M, Fujioka H, Mizuno K, et al. Low-intensity pulsed ultrasound initiates bone healing in rat nonunion fracture model. J Ultrasound Med. 2001;20:197–205.
8. Azuma Y, Ito M, Harada Y, Takagi H, Ohta T, Jingushi S. Low-intensity pulsed ultrasound accelerates rat femoral fracture healing by acting on the various cellular reactions in the fracture callus. J Bone Miner Res. 2001;16:671–80.
9. Jung YJ, Kim R, Ham HJ, Park SI, Lee MY, Kim J, et al. Focused low-intensity pulsed ultrasound enhances bone regeneration in rat calvarial bone defect through enhancement of cell proliferation. Ultrasound Med Biol. 2015;41:999–1007.
10. Cui JH, Park SR, Park K, Choi BH, Min BH. Preconditioning of mesenchymal stem cells with low-intensity ultrasound for cartilage formation in vivo. Tissue Eng. 2007;13:351–60.
11. Takayama T, Suzuki N, Ikeda K, Shimada T, Suzuki A, Maeno M, et al. Low-intensity pulsed ultrasound stimulates osteogenic differentiation in ROS 17/2.8 cells. Life Sci. 2007;80:965–71.
12. Sheyn D, Kimelman-Bleich N, Pelled G, Zilberman Y, Gazit D, Gazit Z. Ultrasound-based nonviral gene delivery induces bone formation in vivo. Gene Ther. 2008;15:257–66.
13. Rubin CT, Lanyon LE. Regulation of bone formation by applied dynamic loads. J Bone Jt Surg Am. 1984;66:397–402.
14. Rubin CT, Lanyon LE. Regulation of bone mass by mechanical strain magnitude. Calcif Tissue Int. 1985;37:411–7.
15. Chen YJ, Wang CJ, Yang KD, Chang PR, Huang HC, Huang YT, et al. Pertussis toxin-sensitive Galphai protein and ERK-dependent pathways mediate ultrasound promotion of osteogenic transcription in human osteoblasts. FEBS Lett. 2003;554:154–8.
16. McPherron AC, Lawler AM, Lee SJ. Regulation of skeletal muscle mass in mice by a new TGF-beta superfamily member. Nature. 1997;387:83–90.
17. Marchitelli C, Savarese MC, Crisa A, Nardone A, Marsan PA, Valentini A. Double muscling in Marchigiana beef breed is caused by a stop codon in the third exon of myostatin gene. Mamm Genome. 2003;14:392–5.
18. Schuelke M, Wagner KR, Stolz LE, Hubner C, Riebel T, Komen W, et al. Myostatin mutation associated with gross muscle hypertrophy in a child. N Engl J Med. 2004;350:2682–8.
19. Zimmers TA, Davies MV, Koniaris LG, Haynes P, Esquela AF, Tomkinson KN, et al. Induction of cachexia in mice by systemically administered myostatin. Science. 2002;296:1486–8.
20. Hamrick MW. Increased bone mineral density in the femora of GDF8 knockout mice. Anat Rec A Discov Mol Cell Evol Biol. 2003;272:388–91.
21. Morissette MR, Stricker JC, Rosenberg MA, Buranasombati C, Levitan EB, Mittleman MA, et al. Effects of myostatin deletion in aging mice. Aging Cell. 2009;8:573–83.
22. Elkasrawy MN, Hamrick MW. Myostatin (GDF-8) as a key factor linking muscle mass and bone structure. J Musculoskelet Neuronal Interact. 2010;10:56–63.
23. Mitchell AD, Wall RJ. In vivo evaluation of changes in body composition of transgenic mice expressing the myostatin pro domain using dual energy X-ray absorptiometry. Growth Dev Aging. 2007;70:25–37.
24. Yarasheski KE, Bhasin S, Sinha-Hikim I, Pak-Loduca J, Gonzalez-Cadavid NF. Serum myostatin-immunoreactive protein is increased in 60–92 year old women and men with muscle wasting. J Nutr Health Aging. 2002;6:343–8.
25. Tang L, Yang X, Gao X, Du H, Han Y, Zhang D, et al. Inhibiting myostatin signaling prevents femoral trabecular bone loss and microarchitecture deterioration in diet-induced obese rats. Exp Biol Med (Maywood). 2016;241:308–16.
26. Funaba M, Ogawa K, Abe M. Expression and localization of activin receptors during endochondral bone development. Eur J Endocrinol. 2001;144:63–71.
27. Hamrick MW, Shi X, Zhang W, Pennington C, Thakore H, Haque M, et al. Loss of myostatin (GDF8) function increases osteogenic differentiation of bone marrow-derived mesenchymal stem cells but the osteogenic effect is ablated with unloading. Bone. 2007;40:1544–53.
28. Bodine PV, Komm BS. Wnt signaling and osteoblastogenesis. Rev Endocr Metab Disord. 2006;7:33–9.
29. Hartmann C. A Wnt canon orchestrating osteoblastogenesis. Trends Cell Biol. 2006;16:151–8.
30. Krishnan V, Bryant HU, Macdougald OA. Regulation of bone mass by Wnt signaling. J Clin Invest. 2006;116:1202–9.
31. Noda T, Nagano H, Takemasa I, Yoshioka S, Murakami M, Wada H, et al. Activation of Wnt/beta-catenin signalling pathway induces chemoresistance to interferon-alpha/5-fluorouracil combination therapy for hepatocellular carcinoma. Br J Cancer. 2009;100:1647–58.
32. Guo W, Flanagan J, Jasuja R, Kirkland J, Jiang L, Bhasin S. The effects of myostatin on adipogenic differentiation of human bone marrow-derived mesenchymal stem cells are mediated through cross-communication between Smad3 and Wnt/beta-catenin signaling pathways. J Biol Chem. 2008;283:9136–45.
33. Kim WK, Choi HR, Park SG, Ko Y, Bae KH, Lee SC. Myostatin inhibits brown adipocyte differentiation via regulation of Smad3-mediated beta-catenin stabilization. Int J Biochem Cell Biol. 2012;44:327–34.
34. Marechal M, Luyten F, Nijs J, Postnov A, Schepers E, van Steenberghe D. Histomorphometry and micro-computed tomography of bone augmentation under a titanium membrane. Clin Oral Implants Res. 2005;16:708–14.
35. Acar AH, Yolcu U, Altindis S, Gul M, Alan H, Malkoc S. Bone regeneration by low-level laser therapy and low-intensity pulsed ultrasound therapy in the rabbit calvarium. Arch Oral Biol. 2016;61:60–5.
36. Angle SR, Sena K, Sumner DR, Virkus WW, Virdi AS. Combined use of low-intensity pulsed ultrasound and rhBMP-2 to enhance bone formation in a rat model of critical size defect. J Orthop Trauma. 2014;28:605–11.
37. Sakurakichi K, Tsuchiya H, Uehara K, Yamashiro T, Tomita K, Azuma Y. Effects of timing of low-intensity pulsed ultrasound on distraction osteogenesis. J Orthop Res. 2004;22:395–403.
38. Shimazaki A, Inui K, Azuma Y, Nishimura N, Yamano Y. Low-intensity pulsed ultrasound accelerates bone maturation in distraction osteogenesis in rabbits. J Bone Jt Surg Br. 2000;82:1077–82.
39. Tis JE, Meffert CR, Inoue N, McCarthy EF, Machen MS, McHale KA, et al. The effect of low intensity pulsed ultrasound applied to

rabbit tibiae during the consolidation phase of distraction osteogenesis. J Orthop Res. 2002;20:793–800.
40. Tang L, Luo K, Liu C, Wang X, Zhang D, Chi A, et al. Decrease in myostatin by ladder-climbing training is associated with insulin resistance in diet-induced obese rats. Chin Med J (Engl). 2014;127:2342–9.
41. Tang L, Gao X, Yang X, Liu C, Wang X, Han Y, et al. Ladder-climbing training prevents bone loss and microarchitecture deterioration in diet-induced obese rats. Calcif Tissue Int. 2016;98:85–93.
42. Tang L, Zhang J, Zhao X, Li N, Jian W, Sun S, et al. Low-intensity pulsed ultrasound promotes exercise-induced muscle hypertrophy. Ultrasound Med Biol. 2017;43:1411–20.
43. Tang L, Li N, Jian W, Kang Y, Yin B, Sun S, et al. Low-intensity pulsed ultrasound prevents muscle atrophy induced by type 1 diabetes in rats. Skelet Muscle. 2017;7:29.
44. Tobita K, Matsumoto T, Ohashi S, Bessho M, Kaneko M, Ohnishi I. Effect of low-intensity pulsed ultrasound stimulation on gap healing in a rabbit osteotomy model evaluated by quantitative micro-computed tomography-based cross-sectional moment of inertia. J Orthop Sci. 2012;17:470–6.
45. Sun JS, Tsuang YH, Lin FH, Liu HC, Tsai CZ, Chang WH. Bone defect healing enhanced by ultrasound stimulation: an in vitro tissue culture model. J Biomed Mater Res. 1999;46:253–61.
46. Zhou S, Schmelz A, Seufferlein T, Li Y, Zhao J, Bachem MG. Molecular mechanisms of low intensity pulsed ultrasound in human skin fibroblasts. J Biol Chem. 2004;279:54463–9.
47. Lim K, Kim J, Seonwoo H, Park SH, Choung PH, Chung JH. In vitro effects of low-intensity pulsed ultrasound stimulation on the osteogenic differentiation of human alveolar bone-derived mesenchymal stem cells for tooth tissue engineering. Biomed Res Int. 2013;2013:269724.
48. Robinson JA, Chatterjee-Kishore M, Yaworsky PJ, Cullen DM, Zhao W, Li C, et al. Wnt/beta-catenin signaling is a normal physiological response to mechanical loading in bone. J Biol Chem. 2006;281:31720–8.
49. Fung CH, Cheung WH, Pounder NM, Harrison A, Leung KS. Osteocytes exposed to far field of therapeutic ultrasound promotes osteogenic cellular activities in pre-osteoblasts through soluble factors. Ultrasonics. 2014;54:1358–65.
50. Harslof T, Frost M, Nielsen TL, Husted LB, Nyegaard M, Brixen K, et al. Polymorphisms of muscle genes are associated with bone mass and incident osteoporotic fractures in Caucasians. Calcif Tissue Int. 2013;92:467–76.
51. Egerman MA, Cadena SM, Gilbert JA, Meyer A, Nelson HN, Swalley SE, et al. GDF11 increases with age and inhibits skeletal muscle regeneration. Cell Metab. 2015;22:164–74.
52. Lu Q, Tu ML, Li CJ, Zhang L, Jiang TJ, Liu T, et al. GDF11 Inhibits bone formation by activating Smad2/3 in bone marrow mesenchymal stem cells. Calcif Tissue Int. 2016;99:500–9.
53. Chen G, Deng C, Li YP. TGF-beta and BMP signaling in osteoblast differentiation and bone formation. Int J Biol Sci. 2012;8:272–88.
54. Inoue Y, Canaff L, Hendy GN, Hisa I, Sugimoto T, Chihara K, et al. Role of Smad3, acting independently of transforming growth factor-beta, in the early induction of Wnt-beta-catenin signaling by parathyroid hormone in mouse osteoblastic cells. J Cell Biochem. 2009;108:285–94.
55. Lerner UH, Ohlsson C. The WNT system: background and its role in bone. J Intern Med. 2015;277:630–49.
56. Lei H, Xin H, Guan R, Xu Y, Li H, Tian W, et al. Low-intensity pulsed ultrasound improves erectile function in streptozotocin-induced type I diabetic rats. Urology. 2015;86(1241):e11–e18.